Polyamidoamine dendrite-tailored mesoporous nanosilica surfaces for high drug loading and controlled release

Hung-Cuong Luu[1, 2], Cuong Quoc Ngo[1, 2], Ngoc Hoi Nguyen[1, 3, 4], Dieu Linh Tran[1, 4], Dai Hai Nguyen[1, 3, 4], Cuu Khoa Nguyen[1*]

[1]Institute of Applied Materials Science, Vietnam Academy of Science and Technology, 01B TL29 Street, Thanh Loc Ward, District 12, Ho Chi Minh City, Vietnam
[2]Biomaterials and Nanotechnology Research Group, Faculty of Applied Sciences, Ton Duc Thang University, 19 Nguyen Huu Tho Street, Tan Phong Ward, District 7, Ho Chi Minh City, Vietnam
[3]Graduate University of Science and Technology, Vietnam Academy of Science and Technology, 18 Hoang Quoc Viet Street, Cau Giay District, Hanoi, Vietnam
[4]Institute of Chemical Technology, Vietnam Academy of Science and Technology, 1A TL29 District 12, Ho Chi Minh City, Vietnam

Received 20 June 2022; accepted 16 September 2022

Abstract:

Mesoporous silica nanoparticles (MSNs) have been demonstrated as a promising candidate in drug delivery applications. With the ambition of enhancing their drug loading capacity and controlled release, in this innovative study, MSNs were tailored with polyamidoamine (PAMAM) dendrimers thereby exerting advantageous properties onto the surface of the nanoplatforms. MSNs were prepared by Stöber's method, sequentially functionalised by amine groups, and respectively grafted with PAMAMs layer-by-layer. Morphology and characterisation of the nanoparticles were carried out through transmission electron microscopy, dynamic light scattering, thermogravimetric analysis, and Fourier-transform infrared spectroscopy. Ninhydrin assay and zeta potential analysis were further employed to investigate the amine-modified nanomaterials. The drug loading and release profiles of particles were also studied. As a result, PAMAM-grafted MSNs, with the highest hydrodynamic size of 185.3 nm, exhibited high encapsulation efficiency (85.8%) and controlled release ability compared to conventional MSNs, suggesting that PAMAM-grafted MSNs would be a promising drug delivery system.

Keywords: **controlled release, drug delivery, mesoporous nanosilica, nanotechnology, polyamidoamine.**

Classification numbers: **2.2, 2.3, 3.6**

1. Introduction

Chemotherapy has become one of the most widely used therapeutics abundantly applied in clinics. However, the treatment of chemotherapy usually requires an excess of chemotherapeutic agents, which inevitably trigger damage to normal tissues [1, 2]. Fortunately, a nanotechnology-mediated approach to chemotherapy has exhibited great potential in enhancing effectiveness by alleviating side effects to healthy tissues and overcoming the drawbacks in the specificity of conventional medicine [3, 4]. With the development of technology, nanomaterials have been well-constructed and designed to improve their pharmacokinetic profile and treatment efficiencies [5]. Besides, with recent insight into the major underlying mechanism--the Enhanced Permeability and Retention (EPR) effect--the "golden age" of nanomedicine was officially born in which a myriad of nanomaterial platforms are being employed for research [6, 7].

Silica-based materials have sparked wide interest with their favourable properties such as chemical and thermal endurance, cytocompatibility, large surface area, and preparedness for surface functionalization [8, 9]. After the invention of Stöber's method based on the sol-gel principle, silica nanoparticles have gained increasing attention [10]. In biomedical applications, nanosilicas are able to be modified in a variety of pathways to become a promising vector for delivering genes [11], antigens [12], proteins [13], and drugs [14, 15], etc. Here, MSNs have emerged at the forefront of silica-based nanomaterials owing to their simple synthesis procedure and architectural control. However, MSNs have several shortcomings that can be enumerated such as the possibility of burst release depending on the interaction between the loaded substances and silica platform and difficulty crossing the epithelial barriers, which could reduce the impact of drugs against disease sites [16, 17]. Nevertheless, these weaknesses could be surmounted by engineered surface modification of MSNs [18, 19].

According to numerous exceptional features, PAMAM dendrimers have emerged as a compatible candidate to overcome the deficiencies of MSNs. PAMAM dendrimers are well-known for their applications in the biomedical field, especially their use in drug delivery [20, 21]. Besides their monodispersity and high aqueous solubility, the polyvalent surface and dendritic architecture, which are similar to biological systems, could augment penetration and functional performance [22, 23]. In addition, the unique hyperbranched structure of PAMAM dendrites generates an interior free-void volume and an exterior of highly dense layers of branches, which could enlarge the loading capacity and decelerate the release rate of drugs. Overall, the combination of PAMAM dendrimers and MSNs could become a novel approach

*Corresponding author: Email: nckhoavnn@yahoo.com

for nanomedicine technology.

In this study, we aimed to engineer conventional MSNs by tailoring PAMAM dendrites on MSN surfaces. The MSNs were synthesised via Stöber's method with nominal modification suggested by our group. The as-synthesised MSNs were further functionalised by amine groups before attaching the PAMAM dendrites. PAMAM grafting was carried out using the Michael reaction and amination reaction, respectively, to attain a third generation of PAMAM dendrimer. To demonstrate its successful preparation, we characterised the morphological and chemical properties of conventional MSNs and a series of PAMAM-modified MSNs by modern methods. The quantification of surface amine groups confirmed the accuracy of synthesis. Finally, with quercetin used as the model drug, the drug loading capacity and release profiles were investigated to validate the enhancement of PAMAM tailoring in comparison with the conventional MSNs in drug delivery ability.

2. Materials and methods

2.1. Materials

Tetraethyl orthosilicate (TEOS, 98%), cetrimonium bromide (CTAB, 98%), (3-aminopropyl)triethoxysilane (APTES, 99%), methyl acrylate (MA, 99%), ethylenediamine (EDA, 99%), ninhydrin (99%), polysorbate 80 (TWEEN 80, 99%), quercetin (QU) (95%), and other reagents were obtained from Merck (Germany). Acid acetic (99.7%) and ammonia (25-28%) were purchased from Xilong (China) Dialysis membrane tubing 12-16 kDa MWCO were purchased from Spectrum™ Labs Spectra/Por™ (USA).

2.2. Methods

The morphology of the particles was observed by scanning electron microscope (SEM, JSM-IT100, Japan) and transmission electron microscope (TEM, JEM-2100, Japan). The obtained SEM image was used to evaluate the mean size of nanoparticles in which ImageJ and Origin software were utilised to perform a size distribution plot. The hydrodynamic size was measured by dynamic light scattering (DLS, SZ-100, Japan), which was also used to determine the zeta potential of nanoparticles. Inherent chemical bonds were detected by Fourier transform-infrared spectrophotometer (FTIR, PerkinElmer, USA) using a KBr pellet. The absorbance measurements of the ninhydrin colorimetric assay were conducted by UV/visible scanning spectrophotometer (UV-Vis, Shimadzu UV-1800, Japan). Thermogravimetric analysis (TGA, Mettler Toledo TGA/DSC 3+, Sweden) was carried out to investigate the thermal stability of particles. The TG plot was recorded from 30 to 800ºC at a ramping rate of 10ºC.min^{-1} under the continuous flow of N_2 gas. X-ray powder diffraction (XRD) patterns were obtained by a diffractometer (Bruker D8 Advance, Germany).

2.3. Synthesis of amine-functionalised MSNs

The fabrication of the MSNs in this research was attempted via the Stöber method with minimal modification as mentioned in a previous publication [24]. The template of this approach was based on the sol-gel process in which TEOS was utilized as the silica precursor, ammonia as the catalyst for hydrolysis and condensation processes, and CTAB as the structure-forming agent. In brief, 2.6 g of CTAB (7.1 mmol) was dissolved in 64 ml of direct ink writing (DIW) and stirred for 30 min to create a homogeneous mixture. The mixture was heated up to 60ºC and the temperature was maintained for 30 min. During this process, the cationic surfactant molecules begin to aggregate to establish spherical micelles. Subsequently, 11.25 ml of EtOH and 550 µl of NH_3 2.8% were added to the above solution and stirred for 5 min at 300 rpm. In this experiment, we used EtOH as the solvent and DIW played a vital role as the reactant in the hydrolysis reaction. Separately, 8 ml of TEOS was transferred to a syringe dispenser and gradually dropped into the resulting solution. The reaction was carried out under vigorous stirring for 2 h at 60ºC. Then, the suspension was quickly cooled down to ambient temperature to terminate the reaction, then sonicated for 30 min. To purify the nanoparticles, the dispersion was dialysed against DIW for 3 h (MWCO 12-14 kDa) and against a mixture of ethanol/ammonia solution (1:1, v/v) for the next 2 d, and finally immersed in DIW for 1 d. After the dialysis process, the MSN-dispersed solution was freeze-dried for further functionalisation.

To chemically activate the surface of the nanoparticles, the inert hydroxyl groups on the spherical surfaces were tailored by amine groups [25]. We utilised the reaction with APTES for the amination of MSNs. Briefly, a suspension of lyophilised MSNs (1 g) in EtOH (20 ml) was gradually introduced into a mixture of APTES and EtOH (1:4, v/v). The reaction was stirred and kept stable at room temperature for 24 h. Ultimately, centrifugation and lyophilization were carried out to collect the amine-functionalised MSNs, which are so-called MSNs-G0.

2.4. Quantitative estimation of amine functional groups

The syntheses of PAMAM dendrites on the silica platforms require high accuracy of the number of moles of reactants; thus, the quantification of the surface concentration of amine is essential for later experiments [26]. We used the ninhydrin test, which is a colorimetric assay based on the reaction of ninhydrin with primary amines to generate a deep purple or blue colour known as Ruhemann's purple. Here, the calibration plot was constructed by preparing a set of highly pristine APTES solutions. The concentration range of the standard substance varied from 50 to 1000 ppm in absolute ethanol solvent. A solution of 0.35% ninhydrin in absolute ethanol (w/v) was carefully prepared and used as an indicator for all quantification assays. Then, 200 mg of functionalised nanoparticles were redispersed in absolute ethanol in a capped vial. Afterwards, the suspensions were placed in a bath sonicator for 30 min; in some cases, the redispersed samples were measured by DLS in order to determine that no aggregation or agglomeration had formed during the purification procedure. Subsequently, 1 ml of the ninhydrin solution was added to the sample-containing vials and placed in a bath sonicator for 10 min,

then transferred to a water bath that was previously set up at 65ºC for 30 min. The resulting dispersions were allowed to cool down to room temperature before undergoing centrifugation to remove the nanoparticles. The supernatant of each sample was pumped out and the absorbance was measured at a wavelength of 588 nm by a Shimadzu UV-1800 UV/visible scanning spectrophotometer. Measurements were conducted three times.

2.5. Synthesis of MSNs-G3

From the nanosilica platform, we developed PAMAM dendrites according to the convergent pathway reported with our nominally adjusted procedure [27, 28]. Briefly, a solution of MA dissolved in methanol was freshly prepared and stirred under nitrogen at 5ºC for 5 min. MSNs-G0 was suspended in a methanol solution and sonicated to be well dispersed. The suspension was added dropwise to the MA solution. After that, the mixture was allowed to react under vigorous stirring and a sealed system at ambient temperature for 4 d. Evaporation and dialysis against methanol were accomplished to eliminate excessive MA and obtain half-generation PAMAM nanoparticles which were denoted by MSNs-G0.5. Sequentially, full-generation PAMAMs were achieved with Michael's reaction. Similarly, a solution of EDA in methanol was also prepared with a blown nitrogen atmosphere at 5ºC for 5 min. A suspension of MSNs-G0.5 in methanol was moderately dropped into the EDA solution. Then, the reaction was carried out under the same conditions with half-generation PAMAM synthesis. Afterwards, unreacted EDA was initially removed *in vacuo* and dialysis against a mixture of toluene/methanol (9:1, v/v) to yield MSNs-G1. The product continually underwent similar routes to attain higher generation PAMAMs, finally stopping at MSNs-G3.

2.6. Loading and release of quercetin

To determine the enhancement in drug loading, an encapsulation of nanomaterials was conducted on the MSNs and MSNs-G3. QU was employed as a typical anticancer compound to evaluate the possibility of these nanosystems in drug delivery. The carriers (10 mg) were dispersed in 9 ml of methanol and ultrasonication was also carried out for 30 min. 1 mg of QU was dissolved in 1 ml of methanol and the solution was then added to the nanomaterial suspensions. The mixtures were allowed to stir overnight in the dark. Subsequently, excessive QU was expelled by the dialysis membrane before lyophilization to yield the drug-encapsulated nanoparticles. These QU-encapsulated were named QU@MSNs and QU@MSNs-G3, respectively. The supernatant containing the excess QU was collected to quantitatively calculate the encapsulation efficiency (%EE) and drug loading capacity (%LC) of the nanomaterials using the following equations:

$$\%EE = \frac{\text{weight of QU in nanoparticles}}{\text{initial weight of QU added}} \times 100\% \quad (1)$$

$$\%LC = \frac{\text{weight of QU in nanoparticles}}{\text{total weight of QU-loaded nanoparticles}} \quad (2)$$

The drug release profile was performed in phosphate buffered saline (PBS) buffer (pH 7.4) including TWEEN 80 (0.5%) at 37ºC using the dialysis method. Then, 2 mg of QU-loaded nanoparticles was dispersed in 2 ml of PBS buffer solution. The suspensions were transferred to dialysis bags (MWCO 12-14 kDa) and sequentially immersed into 18 ml of release medium. The release containers were placed in the dark and maintained at 37ºC until the experiments were completed. At specific intervals, 2 ml of release solution was pipetted out and stored in designated Eppendorf tubes. An equivalent volume of dialysate was refilled. Eventually, the collected samples were measured by UV-Vis spectroscopy at the wavelength of 372 nm to determine the amount of drug released.

2.7. Statistical analysis

All resultant data were illustrated as mean ± standard errors. Statistical evaluation of data was performed by using Student's t-test. A *p*-value smaller than 0.05 was considered statistically significant.

3. Results and discussion

3.1. Morphology and characterisation of MSNs

MSNs were synthesised by Stöber's method using a silicon resource from TEOS and CTAB as a structural platform for the silicon to condense onto. After that, the obtained MSNs were utilised as the starting material for surface modifications.

To determine the particle size and morphology of the silica nanoparticles, SEM and TEM were used (Figs. 1A, B). Basically, both SEM and TEM images showed that the nanosilica particles had a relatively spherical shape with uniform size and no observation of agglomeration or aggregation. By using ImageJ software with the SEM image, the mean size of nanomaterials was calculated as 68.04±5.91 nm (Fig. 1C). This figure could be considered higher than that of previous publications due to our modification in the synthesis route [18]. For the TEM result, the bolder-coloured interior of nanosilica particles was assigned to the silicon-enriched core, which took place during the initial condensation. The outer layer expressed a low density of materials, which consolidated the mesoporous construction of the nanoparticles.

The hydrodynamic diameter of the MSNs was investigated by DLS (Fig. 1D). We utilised a lyophilised nanosilica sample then redispersed it into DIW. The aqueous solution of MSNs was sonicated before the diameters of the particles were measured by scattering light. The DLS measurements were conducted three times with one-minute intervals, which showed that the average size of the nanoparticles in water medium was 135.5±4.5 nm. The resulting data revealed monodispersion in size distribution and colloidal stability of the materials (PDI 0.044) after undertaking dehydration and preservation in advance.

The chemical nature of nanosilica was affirmed by FTIR (Fig. 1D). The typical pattern of silica materials was revealed in the

fingerprint region, in which there was a strong absorbance of the Si-O-Si stretch around the wavelength of 1100 cm^{-1}. For the unmodified MSNs, the FTIR spectrum also showed a broad peak at a little over 3200 cm^{-1}, which was assigned to the hydroxyl groups overexpressed on particles' surfaces. Thus, the FTIR spectrum of MSNs basically confirms the successful synthesis of the nanosilica materials without by-products, excessive reagents, or contaminants. The hydroxyl-overexpressed surface of the MSNs was consolidated by zeta potential measurements as well. The negative isoelectric point was recorded at about -29.9 mV indicating the exposition of acidic -OH groups.

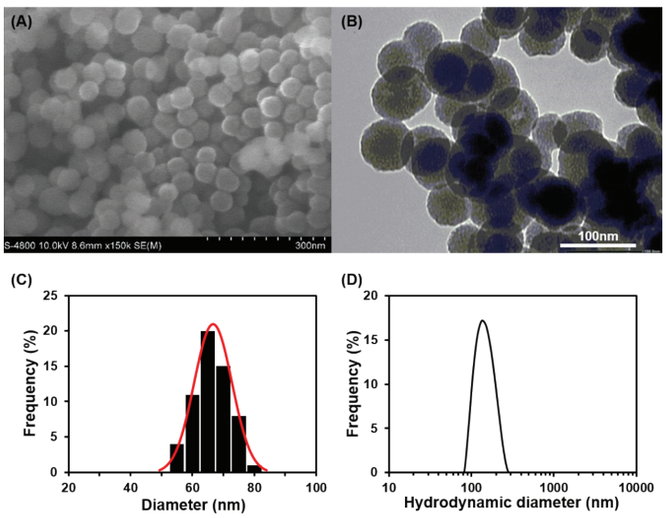

Fig. 1. (A) SEM image and (B) TEM image of MSNs, (C) size distribution computed by ImageJ software, and (D) hydrodynamic size distribution of MSNs.

3.2. Characterisation of MSNs-PAMAM

The series of PAMAM-grafted MSNs were fabricated via step-by-step synthesis routes in which zero-to-three generation PAMAM dendrimers were tailored onto the surface of MSNs (Scheme 1). Firstly, amine groups contained in APTES molecules are decorated on the surface of MSNs in lieu of hydroxyl groups. The amine-functionalised MSNs were employed as reacting cores and denoted by MSNs-G0. MSNs-G0 were reacted with MA via alkylation to obtain MSNs-G0.5, then reacted with EDA via amination to obtain MSNs-G1. The fabrication was respectively carried out with MA and EDA to finally achieve MSNs-G3.

First, DLS was utilised to assess the hydrodynamic sizes and colloidal stability of PAMAM-grafted MSNs (Fig. 2A). The DLS results of the mean hydrodynamic sizes of MSNs-G0, MSNs-G1, MSNs-G2, and MSNs-G3 in DIW were 137.5±4.5 nm, 142.7±4.0 nm, 167.4±4.5 nm, and 185.9±2.5 nm, respectively. In general, the particle sizes significantly increased over a generation, which is consistent with the layer-by-layer structure of PAMAM dendrites. In detail, the size increase between MSNs-G2 and MSNs-G1 showed the highest value at 17.3%, while that between

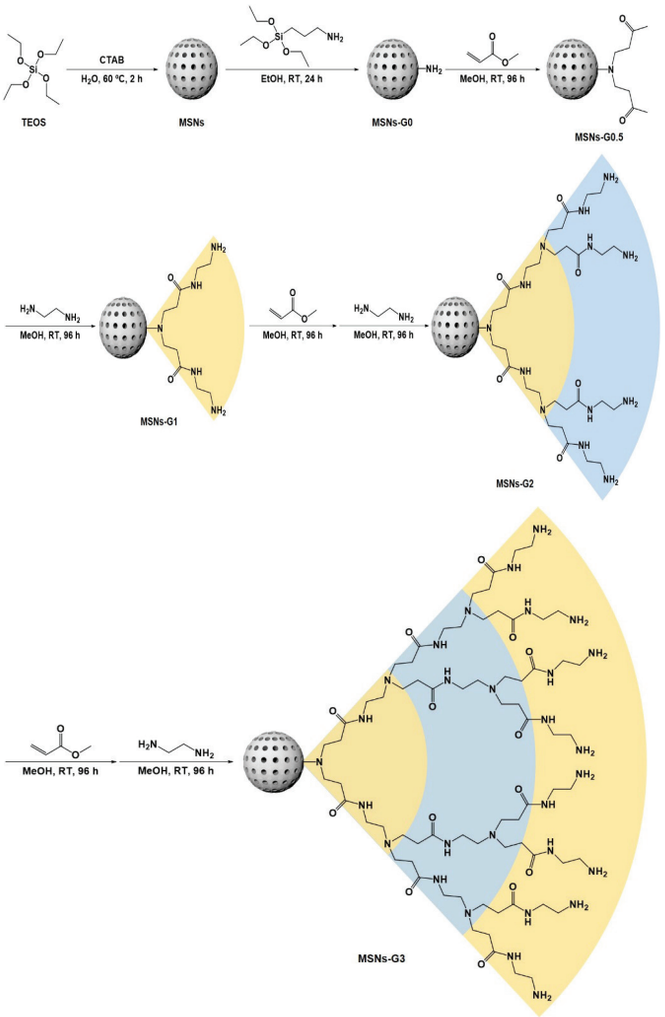

Scheme 1. Synthetic routes of MSNs and PAMAM dendrites-tailored MSNs.

MSNs-G3 and MSNs-G2 was 10.7%. These results demonstrate the shrinkage of the PAMAM structure commencing at the third generation due to the formation of back-folding, which is specifically attributed to the ionization of amide bonds generating an attractive effect between branches [29].

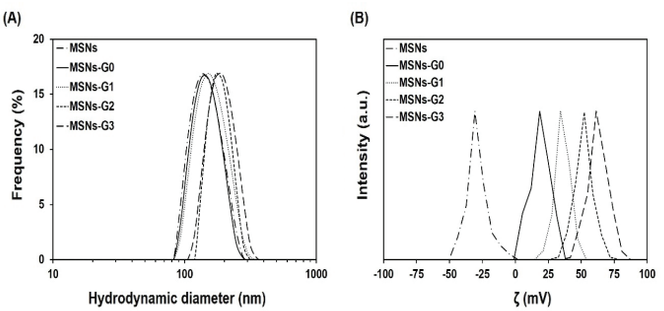

Fig. 2. (A) Hydrodynamic size distributions and (B) zeta potentials of MSNs in comparison with MSNs-PAMAM.

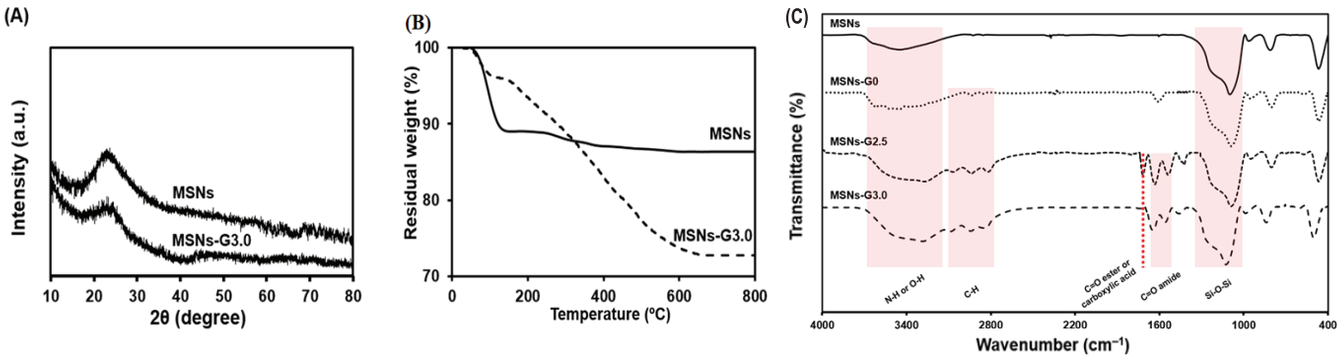

Fig. 3. (A) XRD patterns of MSNs and MSNs-G3.0, (B) thermal decomposition curves of MSNs and MSNs-G3.0, and (C) FTIR spectra of MSNs, MSNs-G0, MSNs-G2.5, and MSNs-G3.0.

In addition, the zeta potentials of nanoparticles were measured under the same conditions including dispersing medium, neutral pH, and particle concentration (Fig. 2B). The graph reveals that the electrokinetic potentials remarkably grew over the increase of PAMAM generations after each synthesis loop, which was attributed to the exponential rise in the number of amine groups attached to the ex-layer.

The thermal decomposition curve was further recorded to prove the successful modification of PAMAM onto the MSN surface (Fig. 3A). We show a comparison of thermograms of MSNs and MSNs-G3 to display the thermal nature of the modified and unmodified materials. For the MSNs plot, there was no evidence of significant degradation in the silica structure up to 800ºC, which confirms the thermal endurance of the silica cores. Notably, MSNs were demonstrated as an efficient adsorbent, which was confirmed by the weight loss of 11.0 wt% of water from 80 to just over 100ºC. Meanwhile, the residual weight of MSNs-G3 was 72.8 wt%, which is comparable to a previous publication [18]. Thus, the greater weight loss of nanomaterial was assigned to organic functionalities of PAMAM, which are easily decompose under high temperatures. Moreover, XRD patterns (Fig. 3B) reveal that MSNs-G3 still behave like an amorphous solid with a unique signal at 22º. Hence, this indicated that there was no change in the non-crystalline structure of MSNs after PAMAM waws modified onto their surface, which also indirectly confirmed that the weight loss occurring in the MSNs-G3 thermogram was only dependent on the attached PAMAM dendrites.

The development of PAMAM dendrites onto the surface of the MSNs was initially validated by FTIR (Fig. 3C). For MSNs-G0, the FTIR spectrum maintained the pattern of silica materials with strong absorption at approximately 1100 cm^{-1}. A broad double trough at the region from 3700 to 3300 cm^{-1} corresponded to adsorption caused by the N-H stretching motion of primary amines. The bending vibration of N-H linkage was also recorded at 1650 cm^{-1} [30]. In addition, the introduction of APTES molecules generated C-H bond stretching signals above 2800 cm^{-1}, which certify the successful functionalisation of the MSNs [31]. From a theoretical viewpoint, the group of half-generation PAMAMs including MSNs-G0.5, MSNs-G1.5, and MSNs-G2.5 or the group of full-generation PAMAMs including MSNs-G1, MSNs-G2, and MSNs-G3 exhibit an analogous pattern due to similarities in terms of chemical structure. Here, the representative spectra of MSNs-G2.5 and MSNs-G3 are presented. According to the Michael reaction with MA, the exposure of ester or carboxylic acid carbonyls was recognised in the band at 1715 cm^{-1} occurring in the spectrum of the half-generation dendrimer. For the full-generation dendrimer, the attachment of EDA eliminated ester carbonyls to form amide carbonyls, which led to the appearance of the specific double band from 1650 to 1550 cm^{-1}. In both half- and full-generation PAMAM dendrimers, the broad trough above 3300 cm^{-1} and amide carbonyl signal remained, which contributed to N-H and C=O stretching within the amide bonds [32]. For the entire synthesis process, silica patterns were observed in all spectra indicating that the silica cores were maintained. Hence, the FTIR spectra demonstrates the consistent grafting of PAMAM onto the surfaces of MSNs.

3.3. Quantification of amine groups of MSNs-PAMAM

The synthesis experiments of PAMAM generally require an excess of reagents to regulate the efficiency of reactions. So, the estimation of amine groups per weight is essential to avoid chemical overconsumption and is a useful tool to gauge reaction efficiency. Ninhydrin analysis was conducted by using a UV-vis spectrometer. Subsequently, the amine concentrations of MSNs-PAMAM were calculated from the intensity of reacted ninhydrin. Assuming there was one -NH_2 group in the MSNs-G0 sample, the molar density of amine groups from ninhydrin analysis was performed in comparison with the theoretical development of PAMAMs over a generation as follows (Table 1).

Table 1. Molar density of amines computed from ninhydrin analysis and zeta potential of nanoparticles.

Specimen	Assumed number of amine groups (*N*, group)	Molar density of amine groups (σ, mmol·g^{-1})	Zeta potential (ζ, mV)
MSNs	0	–	-29.9
MSNs-G0	1	0.617	20.1
MSNs-G1	2	1.351	36.0
MSNs-G2	4	2.649	51.8
MSNs-G3	8	5.207	62.7

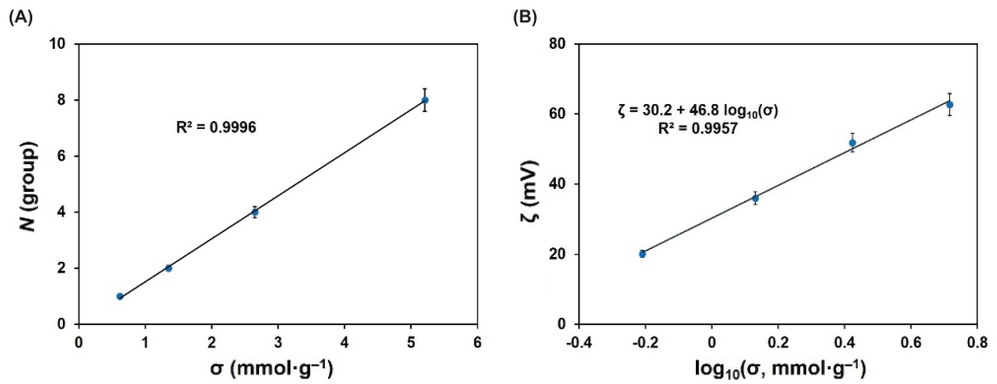

Fig. 4. Linear correlation of (A) molar density versus in the amine number of PAMAM-functionalised MSNs and (B) zeta potential of MSNs-PAMAM versus logarithmic molar density of amine groups.

As can be seen from Table 1, the increase in molar density of -NH_2 groups primarily reveals an exponential growth of PAMAM functionalities by generation. To determine the reaction efficiency, we plotted the molar density of amine groups (σ) as a function of the assumed number of those (Fig. 4A) and assessed the success of synthesis by the linearity of the trend line. Since the correlation coefficient R^2 was 0.9996, the fabrication of MSNs-PAMAM could be recognised as successful with high precision.

We further exploited the positive surface charge of PAMAM dendrites to anticipate the accuracy of modification via the correlation between the zeta potentials (ζ) of colloidal particles and the logarithm of the molar density (σ) (Fig. 4B) [33]. The resultant graph was described by the equation: $\zeta = 30.2+46.8 \log_{10}(\sigma)$ (R^2=0.9957), which demonstrated that the attachments of PAMAM were precise as well.

3.4. Drug loading and release studies

To determine the potential for high drug loading and controlled drug release, we carried out the encapsulation of QU into the PAMAM-grafted MSNs (MSNs-G1 to MSNs-G3) in comparison with conventional MSNs. The encapsulation efficiency (%EE), loading capacity (%LC), and cumulative release amount of QU were calculated following Equations (1) and (2) and are consequently summarized in Table 2. As a general rule, %EE and %LC increased with the generation of PAMAMs implying that the decoration of PAMAM dendrites made an impact on the loading capacity compared to the unmodified MSNs due to empty voids existing in the PAMAM structure.

Table 2. QU loading and cumulative release of QU-encapsulated nanoparticles.

Specimen	%EE	%LC	Cumulative release of QU (%)
QU@MSNs	51.7±0.210	4.7±0.019	85.4±4.4
QU@MSNs-G1	58.4±0.206	5.3±0.019	–
QU@MSNs-G2	76.6±0.109	7.0±0.010	–
QU@MSNs-G3	85.8±0.046	7.8±0.004	70.9±3.9

The drug release profiles were constructed with free drug, QU@MSNs, and QU@MSNs-G3 as a representative for PAMAM-modified MSNs (Fig. 5). For the free drug release profile, QU was rapidly released within 9 hours. By contrast, both MSNs and MSNs-G3 revealed promising potential in controlled release in which QU@MSNs only released 85.4±4.4% within 72 hours and were likely to continue. Meanwhile, the cumulative QU release of QU@MSNs-G3 reached a moderate percentage of 70.9±3.9% and had a saturation tendency, which is attributed to the hyperbranched construction of PAMAM dendrites becoming unintentional drug-capped barriers. However, these results still indicate that higher generation PAMAM remarkably slowed down drug release rate, which could be exploited in drug delivery systems to alleviate side effects that chemotherapeutics trigger.

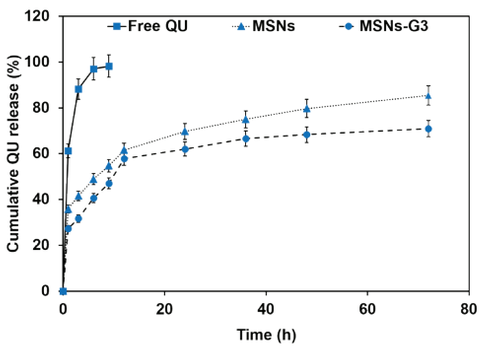

Fig. 5. Drug release profiles of QU@MSNs and QU@MSNs-G3 as compared to free QU in DIW.

4. Conclusions

To conclude, our group successfully synthesised highly monodispersed and spherical MSNs. The modification of PAMAM dendrites onto the surface of silica nanoparticles had outstanding results in which attached PAMAM residues possessed the consistency in chemical structure and appropriate particle sizes for employ as a drug delivery system. Besides, the syntheses of PAMAM-tailored MSNs were obtained with high accuracy and reaction efficiency, which was demonstrated by ninhydrin analysis. A correlation between zeta potential and logarithmic molar density of the amino groups was found, which uncovered a straightforward approach to quickly quantify the fabrication of amine-functionalised nanoparticles. This study initially affirms our viewpoint about the high drug loading capacity and controlled release capability of PAMAM-tailored MSNs to lay the groundwork for further research.

CRediT author statement

Hung-Cuong Luu: Methodology, Software, Conceiving and designing the analysis, Writing- Original draft preparation;

Cuong Quoc Ngo: Data curation, Software; Ngoc Hoi Nguyen: Visualization, Performing the analysis; Dieu Linh Tran: Conceiving and designing the analysis; Dai Hai Nguyen: Validation, Collecting the data, Contributing data or analysis tools; Cuu Khoa Nguyen: Investigation, Conceptualization, Supervision, Writing- Reviewing and Editing.

ACKNOWLEDGEMENTS

This research was funded by the Vietnam National Foundation for Science and Technology (NAFOSTED) under grant no. 104.02- 2019.38.

COMPETING INTERESTS

The authors declare that there is no conflict of interest regarding the publication of this article.

REFERENCES

[1] R. Oun, et al. (2018), "The side effects of platinum-based chemotherapy drugs: A review for chemists", *Dalton Trans.*, **47(19)**, pp.6645-6653.

[2] K. Krukiewicz, J.K. Zak (2016), "Biomaterial-based regional chemotherapy: Local anticancer drug delivery to enhance chemotherapy and minimize its side-effects", *Mater. Sci. Eng. C*, **62**, pp.927-942.

[3] C.Y. Zhao, et al. (2018), "Nanotechnology for cancer therapy based on chemotherapy", *Molecules*, **23(4)**, DOI: 10.3390/molecules23040826.

[4] M.W. Tibbitt, et al. (2016), "Emerging frontiers in drug delivery", *J. Am. Chem. Soc.*, **138(3)**, pp.704-717.

[5] F.D. Cojocaru, et al. (2020), "Nanomaterials designed for antiviral drug delivery transport across biological barriers", *Pharmaceutics*, **12(2)**, DOI: 10.3390/pharmaceutics12020171.

[6] F. Danhier (2016), "To exploit the tumor microenvironment: Since the EPR effect fails in the clinic, what is the future of nanomedicine?", *J. Controlled Release*, **244**, pp.108-121.

[7] D. Kalyane, et al. (2019), "Employment of enhanced permeability and retention effect (EPR): Nanoparticle-based precision tools for targeting of therapeutic and diagnostic agent in cancer", *Mater. Sci. Eng. C*, **98(314)**, pp.1252-1276.

[8] N.T.N. Tram, et al. (2019), "The engineering of porous silica and hollow silica nanoparticles to enhance drug-loading capacity," *Processes*, **7(11)**, DOI: 10.3390/pr7110805.

[9] F. Farjadian, et al. (2019), "Mesoporous silica nanoparticles: Synthesis, pharmaceutical applications, biodistribution, and biosafety assessment", *Chem. Eng. J.*, **359**, pp.684-705.

[10] C. Despas, et al. (1999), "Influence of the base size and strength on the acidic properties of silica gel and monodispersed silica beads: Interest of impedance measurements for the in situ monitoring of the ionization process", *Langmuir*, **15(9)**, pp.3186-3196.

[11] M. Babaei, et al. (2017), "Promising gene delivery system based on polyethylenimine-modified silica nanoparticles", *Cancer Gene Ther.*, **24(4)**, pp.156-164.

[12] T.L. Nguyen, et al. (2020), "Injectable dual-scale mesoporous silica cancer vaccine enabling efficient delivery of antigen/adjuvant-loaded nanoparticles to dendritic cells recruited in local macroporous scaffold", *Biomaterials*, **239**, DOI: 10.1016/j.biomaterials.2020.119859.

[13] G.V. Deodhar, et al. (2017), "Controlled release and intracellular protein delivery from mesoporous silica nanoparticles", *Biotechnol. J.*, **12(1)**, DOI: 10.1002/biot.201600408.

[14] M. Manzano, M. Vallet-Regí (2020), "Mesoporous silica nanoparticles for drug delivery", *Adv. Funct. Mater.*, **30(2)**, DOI: 10.1002/adfm.201902634.

[15] M.C. Ruiz-Cañas, et al. (2020), "Morphological and structural properties of amino-functionalized fumed nanosilica and its comparison with nanoparticles obtained by modified stöber method", *Molecules*, **25(12)**, DOI: 10.3390/molecules25122868.

[16] I.I. Slowing, et al. (2008), "Mesoporous silica nanoparticles as controlled release drug delivery and gene transfection carriers", *Adv. Drug Delivery Rev.*, **60(11)**, pp.1278-1288.

[17] L.M. Kaminskas, et al. (2011), "Dendrimer pharmacokinetics: The effect of size, structure and surface characteristics on ADME properties", *Nanomedicine*, **6(6)**, pp.1063-1084.

[18] B. Wang, et al. (2020), "Poly(amidoamine)-modified mesoporous silica nanoparticles as a mucoadhesive drug delivery system for potential bladder cancer therapy", *Colloids Surf. B*, **189**, DOI: 10.1016/j.colsurfb.2020.110832.

[19] Y. Zhou, et al. (2018), "Mesoporous silica nanoparticles for drug and gene delivery", *Acta Pharm. Sin. B*, **8(2)**, pp.165-177.

[20] M.A. Mintzer, M.W. Grinstaff (2011), "Biomedical applications of dendrimers: A tutorial", *Chem. Soc. Rev.*, **40(1)**, pp.173-190.

[21] I. Grabchev, et al. (2017), "Antimicrobial and anticancer activity of new poly (propyleneamine) metallodendrimers", *J. Polym. Res.*, **24(11)**, pp.1-11.

[22] S. Svenson, D.A. Tomalia (2012), "Dendrimers in biomedical applications-reflections on the field", *Adv. Drug Delivery Rev.*, **64**, pp.102-115.

[23] B. González, et al. (2018), "Mesoporous silica nanoparticles decorated with polycationic dendrimers for infection treatment", *Acta Biomater.*, **68**, pp.261-271.

[24] T.T.N. Thi, et al. (2017), "Hierarchical self-assembly of heparin-PEG end-capped porous silica as a redox sensitive nanocarrier for doxorubicin delivery", *Mater. Sci. Eng. C*, **70(2)**, pp.947-954.

[25] T.N.T. Nguyen, et al. (2019), "Surface PEGylation of hollow mesoporous silica nanoparticles via aminated intermediate", *Prog. Nat. Sci. Mater. Int.*, **29(6)**, pp.612-616.

[26] Y. Sun, et al. (2019), "Quantification of amine functional groups on silica nanoparticles: A multi-method approach", *Nanoscale Adv.*, **1(4)**, pp.1598-1607.

[27] D.T.D. Nguyen, et al. (2019), "Preparation and characterization of oxaliplatin drug delivery vehicle based on PEGylated half-generation PAMAM dendrimer", *J. Polym. Res.*, **26(5)**, pp.1-14.

[28] M.N. Ho, et al. (2019), "PEGylated PAMAM dendrimers loading oxaliplatin with prolonged release and high payload without burst effect", *Biopolymers*, **110(7)**, DOI: 10.1002/bip.23272.

[29] P.K. Maiti, et al. (2005), "Effect of solvent and pH on the structure of PAMAM dendrimers", *Macromolecules*, **38(3)**, pp.979-991.

[30] M. Khoeini, et al. (2019), "Improvement of hollow mesoporous silica nanoparticles synthesis by hard-templating method via CTAB surfactant", *Ceramics International*, **45(10)**, pp.12700-12707.

[31] P. Larkin (2017), *Infrared and Raman Spectroscopy: Principles and Spectral Interpretation*, Elsevier, 286pp.

[32] M.T. Vu, et al. (2016), "Modified carboxyl-terminated PAMAM dendrimers as great cytocompatible nano-based drug delivery system", *International Journal of Molecular Sciences*, **20(8)**, DOI: 10.3390/ijms20082016.

[33] E. Soto-Cantu, et al. (2012), "Synthesis and rapid characterization of amine-functionalized silica", *Langmuir*, **28(13)**, pp.5562-5569.